Electronic Supplementary Material (ESI) for Materials Horizons.

Electronic supplementary information for

Flexo-photoelectronic effect in *n*-type/*p*-type two-dimensional semiconductors and a deriving light-stimulated artificial synapse

Xiang Wang, Xin Zhou, Anyang Cui, Menghan Deng, Xionghu Xu, Liping Xu, Yan Ye, Kai Jiang, Liyan Shang, Liangqing Zhu, Jinzhong Zhang, Yawei Li, Zhigao Hu, and Junhao Chu

Correspondence to: aycui@phy.ecnu.edu.cn; zghu@ee.ecnu.edu.cn

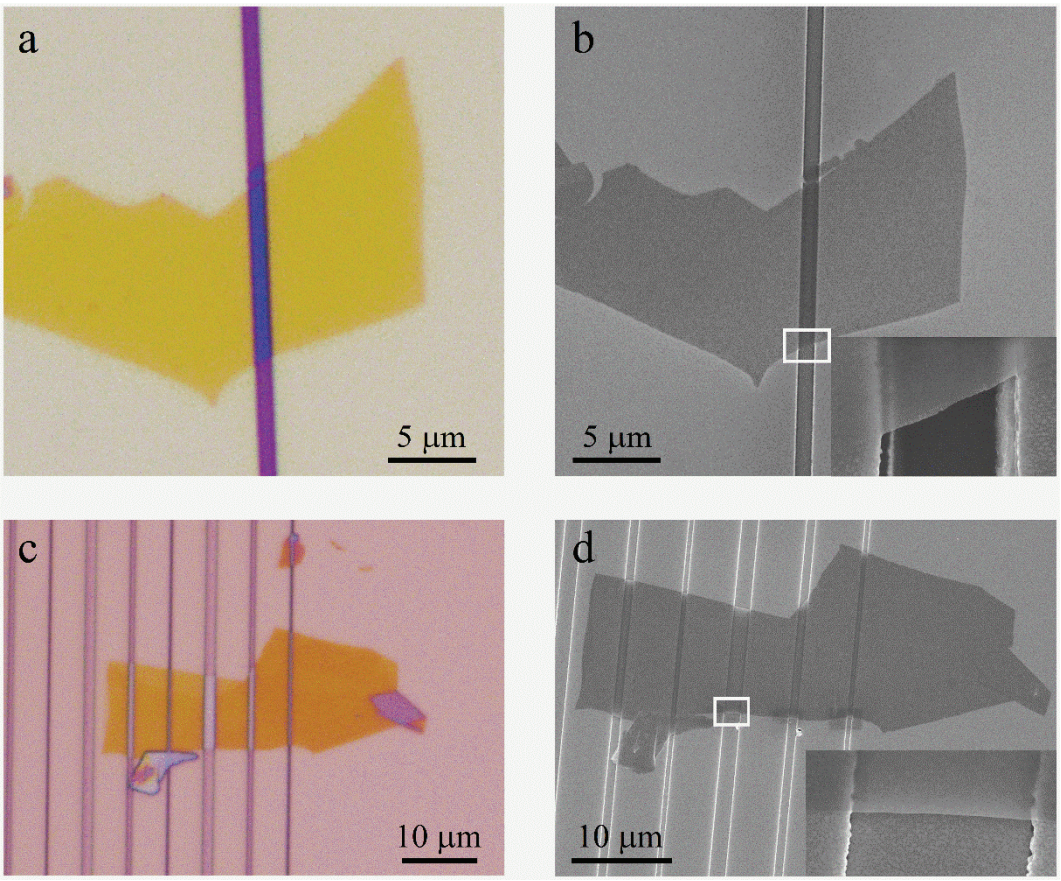

Figure S1 | Optical and SEM images of few-layered InSe flakes suspended on the channel-patterned substrates. Optical **(a)** and SEM **(b)** images of InSe few-layer covering on a channel with width about 1 μm. Optical **(c)** and SEM **(d)** images of InSe few-layer covering on arrayed channels, whose widths are set at 0.75 μm, 1 μm and 1.5 μm, respectively. Both the optical and SEM images clearly show the homogeneous and undamaged quality of transferred InSe flakes. The high-resolution SEM images inset in **(b)** and **(d)** indicate the suspended InSe few-layer at the channel regions.

Note S1 | The contribution of instrinc in-plane piezoelectricity in the PFM response.

In PFM measurements, in addition to the response originated from the flexoelectric effect, the projection in the z direction of intrinsic in-plane piezoelectric response may also be collected, owing to the inflection of 2D materials. By rough calculation, it can be found that the projection of the intrinsic in-plane piezoelectric coefficient (d_{11}) along the z direction contributes very little to the measured effective out-of-plane piezoelectric coefficient. As shown in revised Fig. S2, the cross section of bent 2D materials can be approximated as a circular arc. The projection in the z direction of intrinsic in-plane piezoelectric coefficient ($d_{11,z}$) could be defined as $d_{11,z} = d_{11}\sin\theta$. Obviously, the projection in the z direction of intrinsic in-plane piezoelectric coefficient ($d_{11,z}$) is zero at the center (point M) and maximized at the endpoint (point P). Thus, the measured maximum of d_{33}^{eff} (about 9.5 pm/V) at the center of bent-InSe channel is all the contribution of flexoelectric polarization. In our experiment, the depth and width of the bent-InSe channel are about 50 nm and 1um, respectively. Geometrically, it is easy to conclude that the maximum of $\sin\theta$ is about 0.2 at point P. Theoretically, the intrinsic in-plane piezoelectric coefficient (d_{11}) of 2D InSe obtains the maximum of about 1.98 pm/V at single layer[1]. Hence, the maximum of $d_{11,z}$ is less than 0.396 pm/V at the point P, which is negligible compared to the measured d_{33}^{eff} (about 5.5 pm/V) at the edge of bent-InSe channel. Thereby, it can be concluded that the d_{33}^{eff} of bent 2D InSe dominantly comes from the flexoelectric efffect rather than the instrinc in-plane piezoelectricity.

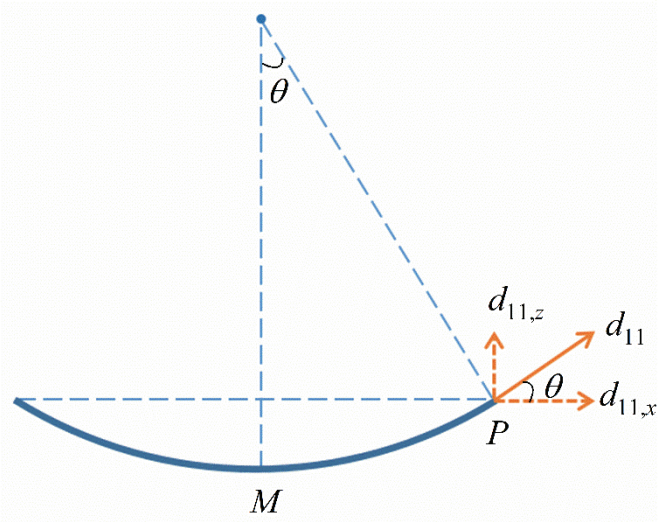

Figure S2 | The decomposition of intrinsic in-plane piezoelectric coefficient of bent 2D materials

Note S2 | Flexoelectric polarization and flexo-phtoelectronic effect of bent WSe_2 few-layer.

In order to quantify the flexoelectric effect of bent WSe_2 few-layer, the PFM measurements were carefully performed with the ascending AC drive voltage from 0 to 5 V at a step size of 0.5 V, as shown in Figure S3. The WSe_2 few-layer was naturally dropt at the suspended region (see Figure S3a). At suspended region, PFM amplitude apparently enhanced with the increasing drive voltage (see Figures S3b, 3c and 3d), consisting with the PFM results of InSe few-layer illustrated in Figure 2 of our manuscript. The WSe_2 channel shows a mirror-type symmetrical morphology with the width of about 1 μm and depth of about 80 nm in the suspended region (see Figure S3e). As a common method, the d_{33}^{eff} coefficient can be calculated by plotting the PFM amplitude as the function of drive voltage amplitude (see Figure 2d of our manuscript; also see ref. 2). The d_{33}^{eff} coefficients also show a mirror-type symmetrical distribution in the bent channel with the maximum value about 4.9 pm/V at the center (see Figure S3f). The PFM findings of suspended WSe_2 are similar to those of suspended InSe indicate that flexoelectric effect induced by strain-gradient universally exist in bent 2D semiconductor materials.

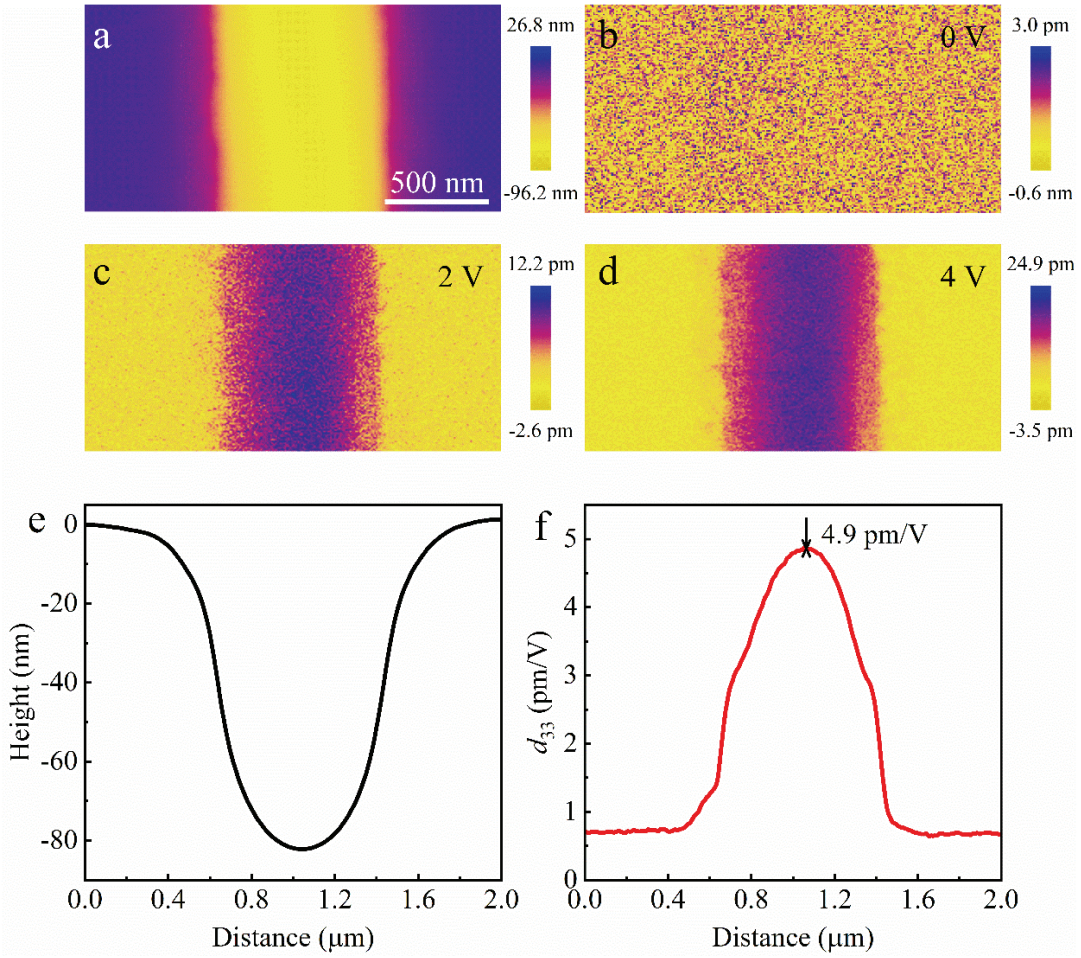

Figure S3 | PFM characterization of the bent WSe_2-based device (**a**) Surface morphology of suspended WSe_2 flake collected by AFM. The out-of-plane (OOP) PFM amplitude images of suspended WSe_2 channel under the ascending drive voltage of **(b)** 0 V, **(c)** 2 V, and **(d)** 4 V, respectively. **(e)** The line profile of morphology along the direction perpendicular to the channel. **(f)** The distribution of d_{33}^{eff} coefficients along the direction perpendicular to the channel.

The flexoelectric polarization not only could induce the redistribution of charge in bent 2D semiconductors, but also regulate the transport behavior of photogenerated charge carriers.[3,4] Additionally, the flexo-phoelectric effect might be different in n-type InSe and p-type WSe_2. Thus, we carried out the same lighting-KPFM tests on the representative InSe-based device and WSe_2-based device, respectively. The data of InSe-based device and WSe_2-based device are exhibited in Figure 3 of our manuscript and Figure S4, respectively. In dark case, the surface potential of channel center is more than 600 mV higher than that of flat region (see Figure S4a), indicating that work function of WSe_2 decreases over 600 meV after bending.[5] It might be related to the accumulation of positive charges at the channel center. On the contrary, negative charges are localized at the channel center after bending in InSe-based device. Thus, there is a potential barrier (see Figure S4a) and a potential well (see Figure 3a of our manuscript) induced by bending at the WSe_2 channel and InSe channel, respectively. Furthermore, under the laser illumination, photogenerated electrons/holes are trapped by the barrier/well, resulting in the depression/enhancement on surface potential of WSe_2/InSe channel with the increasing laser intensity (see Figure S4 and Figure 3 of our manuscript). Under the action of light field, the opposite evolutions of surface potential in InSe- and WSe_2-based devices clearly illustrate the contrary expression of flexo-phoelectric effect in n-type and p-type semiconductors.

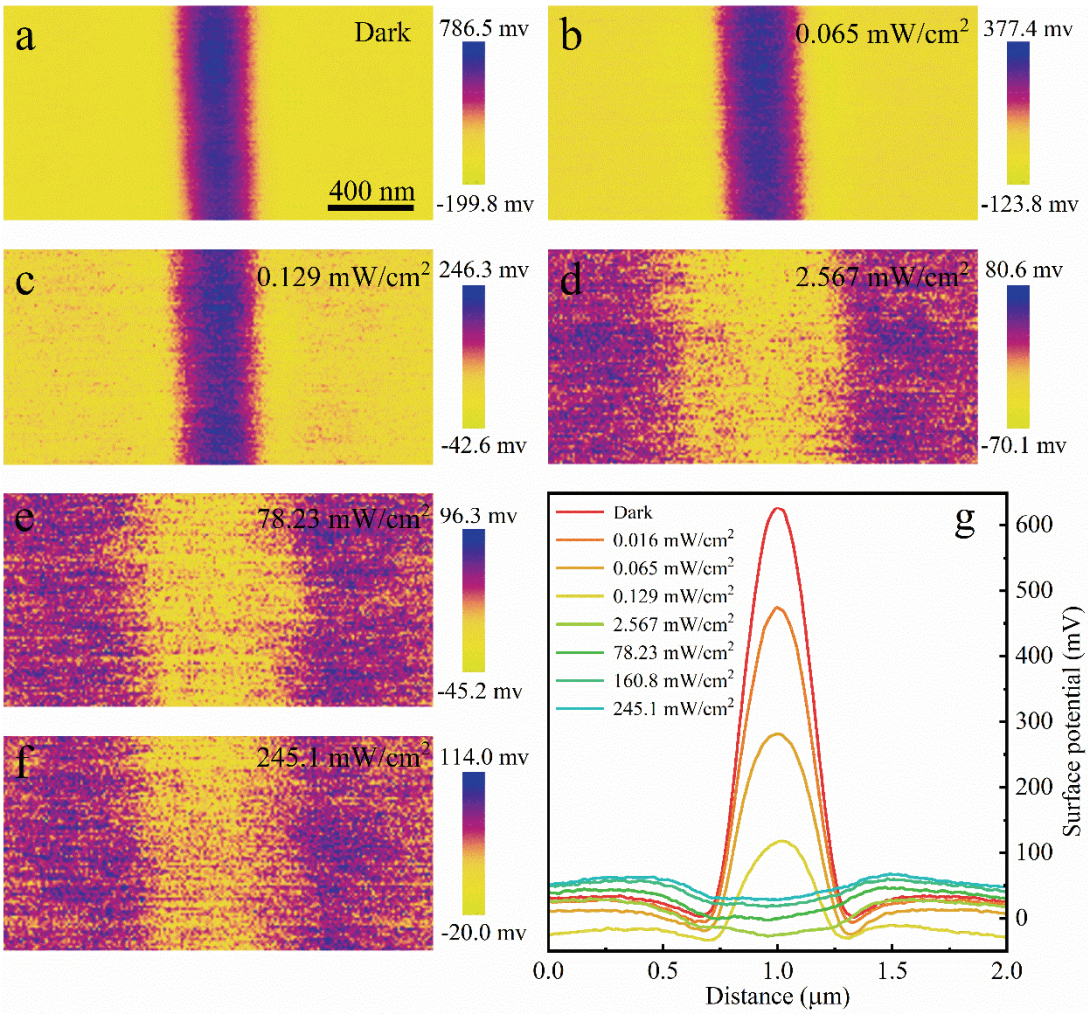

Figure S4 | The lighting-KPFM measurements of the bent WSe_2-based device. The surface potential images of bent WSe_2 channel under **(a)** the dark and under the 405 nm laser with the

intensity of **(b)** 0.065 mW/cm^2, **(c)** 0.129 mW/cm^2, **(d)** 2.567 mW/cm^2, **(e)** 78.23 mW/cm^2 and **(f)** 245.1 mW/cm^2. **(g)** The surface potential distribution along the direction perpendicular to channel under the different illumination.

Note S3 | *I-V* curves of the representative bent-InSe device in dark and in continuous illumination.

As shown in Fig. S5, the I_{ds}-V_{ds} curves of the bent-InSe device under darkness and various irradiation intensities of a 405 nm laser are symmetric and linear, which is consistent with the symmetric structure of the device. A significant enhancement of photocurrent ($I_{ph} = I_{light} - I_{dark}$) at a fixed bias is observed as the laser irradiation intensity (P_{in}) increases. It is attributed to that the number of photo-generated carriers increase. As is known, responsivity (R_{ph}) and detectivity (D^*) are two key figures of merits of photoelectric device. R_{ph} represents the efficiency of the device in response to the incident light, which can be extracted from the formula $R_{ph} = \frac{I_{ph}}{P_{in}A}$, where A is the effective area (about 10 μm^2). D^* represents the sensitivity of the detector, $D^* = \frac{R_{ph}A^{1/2}}{(2qI_{dark})^{1/2}}$, where q is the electron charge and I_{dark} is the dark current. At the fixed bias of 0.1 V, the maximum values of R_{ph} and D^* can reach up to 288.7 A/W and 2.45 × 10^{12} Jones, respectively, under an ultralow laser power of ~ 0.065 mW/cm^2. The R_{ph} and D^* of our device are slightly better than previously reported results (with R_{ph} = 157 A/W and D^* ~ 10^{11} Jones) in traditional InSe phototransistor[6].

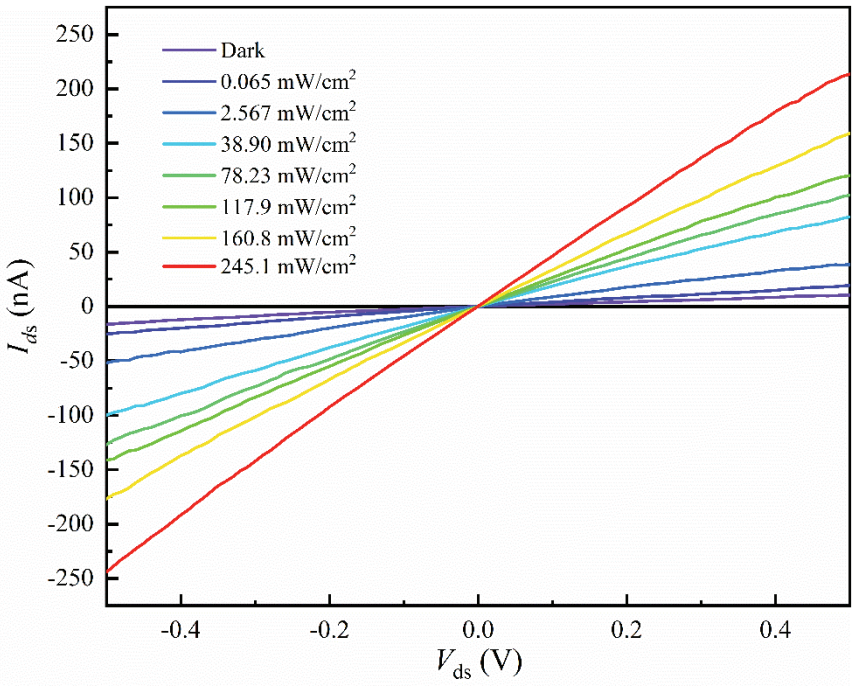

Figure S5 | I-V curves of the representative bent-InSe device in dark and in continuous illumination.

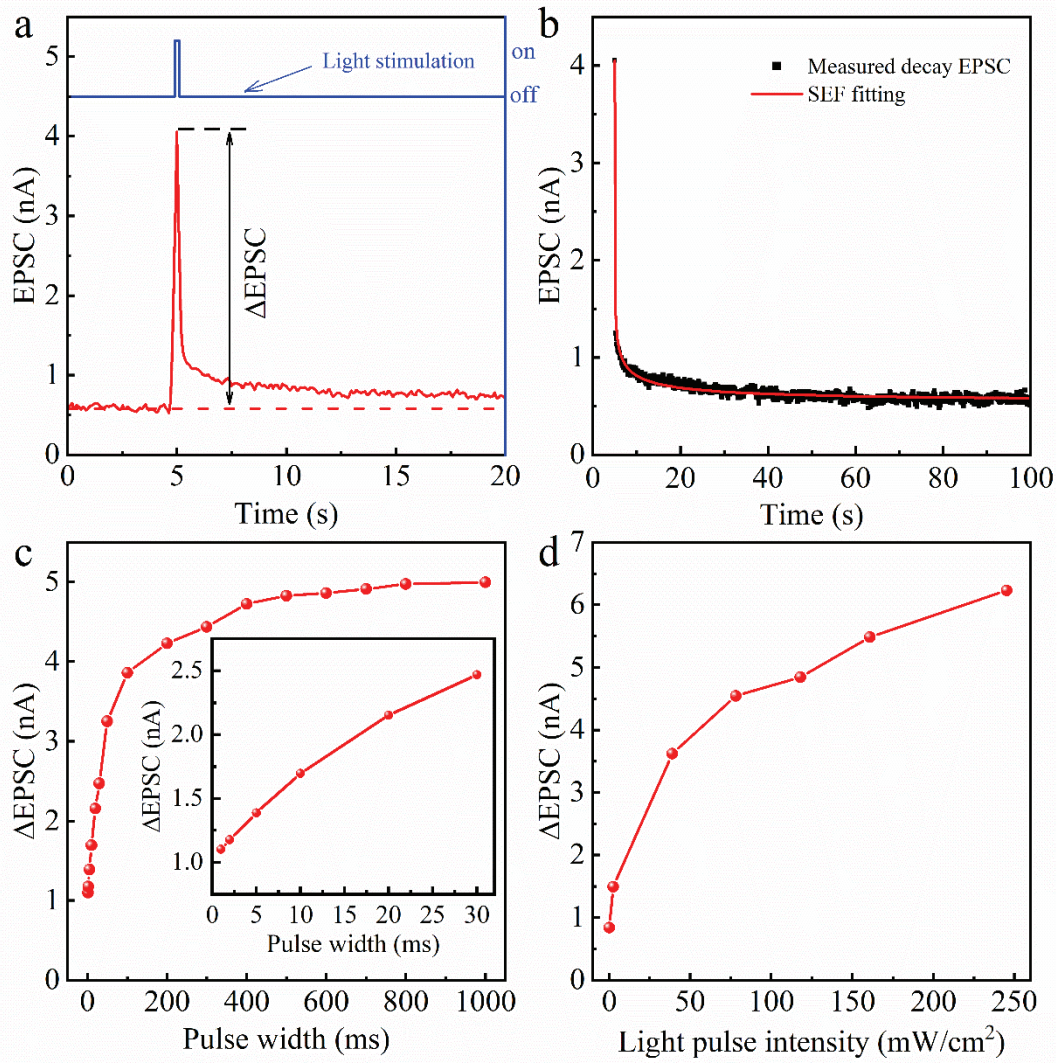

Figure S6 | EPSC characterization of the artificial synapse. (a) Typical EPSC triggered by a presynaptic light pulse (405 nm, 38.9 mW/cm^2, 200 ms). **(b)** EPSC retention curve fitted by the stretched exponential function (SEF). **(c)** The light pulse width-dependent EPSC change (ΔEPSC), defined as the difference between the EPSC at the end of light pulse and the initial current before any light stimulus. **(d)** The light pulse intensity-dependent ΔEPSC. The reading bias is fixed at 0.1 V in all EPSC measurements.

Note S4 | The controlled experiments on flat InSe devices.

In the controlled trials, the InSe channel is flatted on the Si/SiO_2 substrate without bending. The corresponding EPSC characterization is depicted in Figure S7. As shown in Fig. S7b and S7c, the current increases periodically in response to the light pulse but falls to its initial level soon after the light pulse stops. Apparently, although the flat InSe device also possesses conspicuous photocurrent, but it does not exhibit the persistent photoconductivity. Compared with the correlative results of bent InSe device in Fig. 6d and 6f of our manuscript, it can be concluded that the persistent photoconductivity of bent-InSe device mainly comes from the contribution of the bent band rather than the contribution of the defect.

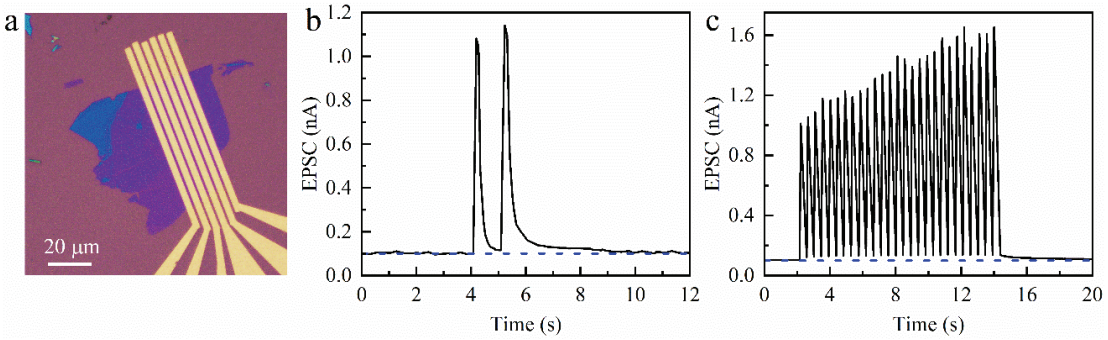

Figure S7 | EPSC characterization of the flat InSe device. (a) Optical image of the flat InSe device supported by the silicon wafers with 300 nm SiO_2 layer. **(b)** EPSC trigged by a pair of light spikes (405 nm, 38.9 mW/cm^2, 200 ms) with a fixed reading bias of 0.1 V. **(c)** EPSC trigged by thirty consecutive light spikes with a fixed reading bias of 0.1 V.

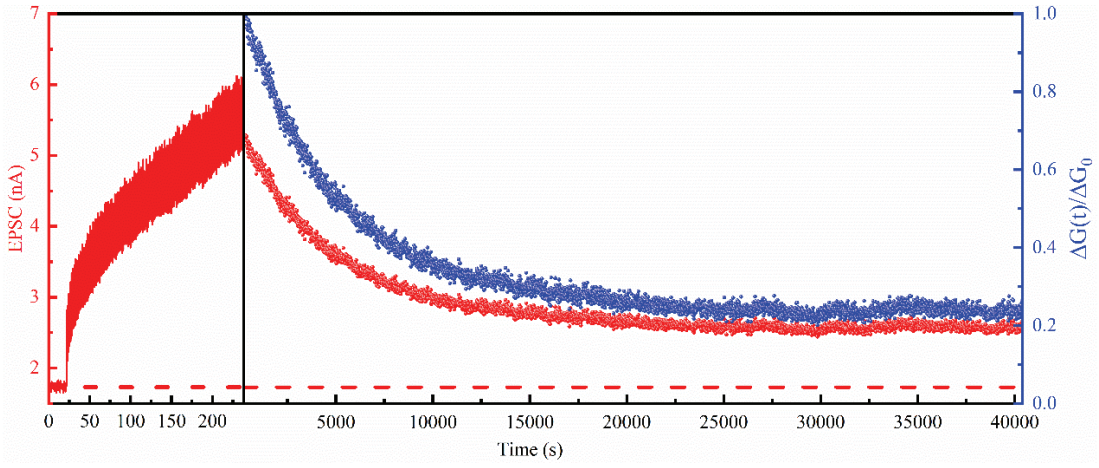

Figure S8 | Long-term memory behavior of light-stimulated artificial synapse after 200 successive light spikes (405 nm, 38.9 mW/cm^2, 200 ms).

References

1. Y. Guo, S. Zhou, Y. Z. Bai and J. J. Zhao, *Appl. Phys. Lett.*, 2017, **110**, 163102.
2. N. Syed, A. Zavabeti, J. Z. Ou, M. Mohiuddin, N. Pillai, B. J. Carey, B. Y. Zhang, R. S. Datta, A. Jannat, F. Haque, K. A. Messalea, C. Xu, S. P. Russo, C. F. McConville, T. Daeneke and K. Kalantar-Zadeh, *Nat. Commun.*, 2018, **9**, 3618.
3. L. F. Wang, S. H. Liu, X. L. Feng, C. L. Zhang, L. P. Zhu, J. Y. Zhai, Y. Qin and Z. L. Wang, *Nat. Nanotechnol.*, 2020, **15**, 661.
4. J. Lu, J. Yao, J. Yan, W. Gao, L. Huang, Z. Zheng, M. Zhang and J. Li, *Mater. Horiz.*, 2020, **7**, 1427-1435.
5. K. Zhang, T. Zhang, G. Cheng, T. Li, S. Wang, W. Wei, X. Zhou, W. Yu, Y. Sun, P. Wang, D. Zhang, C. Zeng, X. Wang, W. Hu, H. J. Fan, G. Shen, X. Chen, X. Duan, K. Chang and N. Dai, *ACS Nano*, 2019, **10**, 3852-3858.
6. S. R. Tamalampudi, Y. Y. Lu, U. R. Kumar, R. Sankar, C. D. Liao, B. K. Moorthy, C. H. Cheng, F. C. Chou, and Y. T. Chen, *Nano Lett.*, 2014, **14**, 2800-2806.